AD-A152 331   COMPUTATION OF VELOCITY AND PRESSURE VARIATION ACROSS AXISYMMETRIC THICK..(U) DAVID W TAYLOR NAVAL SHIP RESEARCH AND DEVELOPMENT CENTER BET.. T T HUANG ET AL.   1/1

UNCLASSIFIED   MAR 85 DTNSRDC-85-014   F/G 20/4   NL

END

FILMED

DTIC

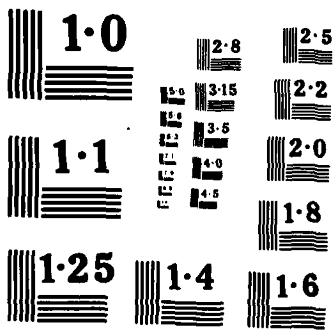
1·0
2·8
2·5
3·15
2·2
3·5
2·0
4·0
1·1
4·5
1·8
1·25
1·4
1·6

UNCLASSIFIED
SECURITY CLASSIFICATION OF THIS PAGE

REPORT DOCUMENTATION PAGE

1a REPORT SECURITY CLASSIFICATION UNCLASSIFIED	1b RESTRICTIVE MARKINGS
2a SECURITY CLASSIFICATION AUTHORITY	3 DISTRIBUTION/AVAILABILITY OF REPORT APPROVED FOR PUBLIC RELEASE: DISTRIBUTION UNLIMITED
2b DECLASSIFICATION/DOWNGRADING SCHEDULE	
4 PERFORMING ORGANIZATION REPORT NUMBER(S) DTNSRDC-85/014	5 MONITORING ORGANIZATION REPORT NUMBER(S)
6a NAME OF PERFORMING ORGANIZATION David W. Taylor Naval Ship R&D Center 6b OFFICE SYMBOL (If applicable) Code 1542	7a NAME OF MONITORING ORGANIZATION
6c ADDRESS (City, State, and ZIP Code) Bethesda, Maryland 20084-5000	7b ADDRESS (City, State, and ZIP Code)
8a NAME OF FUNDING/SPONSORING ORGANIZATION 8b OFFICE SYMBOL (If applicable)	9 PROCUREMENT INSTRUMENT IDENTIFICATION NUMBER
8c ADDRESS (City, State, and ZIP Code)	10 SOURCE OF FUNDING NUMBERS

PROGRAM ELEMENT NO	PROJECT NO	TASK NO	WORK UNIT ACCESSION NO
61152N		ZR 0230101	(Over)

11 TITLE (Include Security Classification)
COMPUTATION OF VELOCITY AND PRESSURE VARIATION ACROSS AXISYMMETRIC THICK TURBULENT STERN FLOWS

12 PERSONAL AUTHOR(S)
Thomas T. Huang and Ming-Shun Chang

13a TYPE OF REPORT	13b TIME COVERED	14 DATE OF REPORT (Year, Month, Day)	15 PAGE COUNT
Final	FROM ____ TO ____	March 1985	29

16 SUPPLEMENTARY NOTATION
Presented at the Third Symposium on Numerical and Physical Aspects of Aerodynamic Flows, California State University, Long Beach, California, 21-24 January 1985

17 COSATI CODES		
FIELD	GROUP	SUB-GROUP

18 SUBJECT TERMS (Continue on reverse if necessary and identify by block number)
Thick turbulent stern flows, boundary layer, turbulence modeling, viscous-inviscid flow interaction, axisymmetric flows.

19 ABSTRACT (Continue on reverse if necessary and identify by block number)

When the curvature of a ships surface is large and the stern boundary layer is thick the cross-stream inviscid velocity and pressure variation becomes important in stern boundary layer computations. The second momentum equation is of the form

$$\frac{\partial p}{\partial n} = \kappa \rho u^2$$

where κ is the curvature of the stern flow, which is different from the surface curvature of the body, u is the velocity along a streamline, p is the pressure, and ρ is the mass density of the fluid. Two viscous-inviscid interaction computation procedures are presented. One uses a marching technique in a natural streamline coordinate system together with the k-ε turbulence model to solve the axisymmetric Reynolds-averaged

(Continued on reverse side)

20 DISTRIBUTION/AVAILABILITY OF ABSTRACT ☒ UNCLASSIFIED/UNLIMITED ☐ SAME AS RPT ☐ DTIC USERS	21 ABSTRACT SECURITY CLASSIFICATION UNCLASSIFIED
22a NAME OF RESPONSIBLE INDIVIDUAL Dr. Thomas T. Huang	22b TELEPHONE (Include Area Code) (202) 227-1325 22c OFFICE SYMBOL Code 1542

UNCLASSIFIED

SECURITY CLASSIFICATION OF THIS PAGE

(Block 10): Work Unit
Accession No.

1542-103
1542-140

(Block 19 continued)

parabolized Navier-Stokes equations for the streamline velocity u, flow angle α, curvature κ, and hence the pressure (p). The numerical procedure starts at a station on the body where the boundary layer is thin and marches downstream into the wake. The boundary conditions for the values of u and p over the inlet plane and along a cylindrical stream surface outside the boundary layer/wake are set by the appropriate values obtained from the other simple viscous-inviscid interaction computations using a modified thin boundary layer method and potential flow calculations about an equivalent displacement body. Comparisons are made between the numerical results and the experimental data for four different sterns. Comparisons of measured axial and radial velocity and pressure distributions and those computed by the simple interaction approximations and partially parabolized techniques have been made. The simple and efficient viscous-inviscid procedure for the computation of velocity and pressure variations across thick turbulent stern flows has been shown to be accurate enough to use as a preliminary design tool.

Originator-supplied key words included: [illegible]

NTI
DTI
Av
Dist

A-1

UNCLASSIFIED

SECURITY CLASSIFICATION OF THIS PAGE

TABLE OF CONTENTS

LIST OF FIGURES

ADMINISTRATIVE INFORMATION

The work described in this paper was funded under the David W. Taylor Naval Ship Research and Development Center's Independent Research Program, Program Element 61152N, Task Area ZR 0230101 and DTNSRDC Work Unit 1542-103 (FY-84) and -140 (FY-85).

COMPUTATION OF VELOCITY AND PRESSURE VARIATION ACROSS AXISYMMETRIC THICK TURBULENT STERN FLOWS

By

Thomas T. Huang and Ming-Shun Chang
David W. Taylor Naval Ship Research and Development Center
Bethesda, Maryland 20084

Abstract

When the curvature of a ships surface is large and the stern boundary layer is thick the cross-stream inviscid velocity and pressure variation becomes important in stern boundary layer computations. The second momentum equation is of the form

$$\frac{\partial p}{\partial n} = \kappa \rho u^2$$

where κ is the curvature of the stern flow, which is different from the surface curvature of the body, u is the velocity along a streamline, p is the pressure, and ρ is the mass density of the fluid. Two viscous-inviscid interaction computation procedures are presented. One uses a marching technique in a natural streamline coordinate system together with the k-ϵ turbulence model to solve the axisymmetric Reynolds-averaged parabolized Navier-Stokes equations for the streamline velocity u, flow angle α, curvature κ, and hence the pressure p. The numerical procedure starts at a station on the body where the boundary layer is thin and marches downstream into the wake. The boundary conditions for the values of u and p over the inlet plane and along a cylindrical stream surface outside the boundary layer/wake are set by the appropriate values obtained from the other simple viscous-inviscid interaction computations using a modified thin boundary layer method and potential flow calculations about an equivalent displacement body. Comparisons are made between the numerical results and the experimental data for four different sterns. Comparisons of measured axial and radial velocity and pressure distributions and those computed by the simple interaction approximations and partially parabolized techniques have been made. The simple and efficient viscous-inviscid procedure for the computation of velocity and pressure variations across thick turbulent stern flows has been shown to be accurate enough to use as a preliminary design tool.

I. Introduction

Many propellers and appendages are located inside of ship stern boundary layers. Therefore, it is essential for naval designers to obtain a fundamental understanding and an accurate predictions of this special class of external thick turbulent stern flows. A series of experiments has been conducted at David W. Taylor Naval Ship R&D Center to determine the unique turbulence structure and viscous-inviscid interaction of thick axisymmetric {1,2,3,4} and simple three-dimensional {5,6,7} stern flows. The Lighthill {8} displacement body concept has been proven experimentally to be an accurate approach for computing viscous-inviscid stern flow interaction. The measured static pressure distributions on the body and across the entire boundary layers were predicted by the displacement body method to an accuracy within one percent of dynamic pressure.

Neither the measured values of eddy viscosity nor the mixing length were found to be proportional to the local displacement thickness or the local boundary-layer thickness of the thick axisymmetric boundary layer. The measured mixing length of the thick stern boundary layer was found to be proportional to the square root of the local cross-section area of the turbulence region [9]. This simple similarity hypothesis for the mixing length and the displacement body concept has been incorporated into the Douglas C-S differential boundary-layer method {10} by Wang and Huang {11}. The method predicts satisfactorily the measured mean velocity distributions for the boundary layer flows of five sets widely different axisymmetric body shapes and has been used as a reliable design tool.

Nakayama, Patel, and Landweber {12, 13}, and Dyne {14} do not use the displacement body method to solve the interaction problem. In all of the methods, the flow field is divided into an inner viscous region composed of all or part of the flow in the body/wake domain and an outer potential flow region. Differences arise in the equations used to solve the viscous flow and the manner of defining the inner and outer regions. Dyne uses the integral approach of Head {15} to calculate the boundary layer flow over the forebody. Over the stern of the body and in the near wake, he uses a differential approach which approximately accounts for the curvature and normal pressure variation effects. An important feature of his approach is that the boundary layer equations are solved along streamlines, which leads to a simplification in the form of the equation. Also, no distinction needs to be made between flow over the body and in the wake. In the approach by Nakayama, Patel, and Landweber, integral relations involving conservation of momentum and continuity are used to relate the momentum area and stream function at the body-wake junction. Patel and Lee {16} present some results for a differential approach which includes all of the curvature effects. A modified displacement-body method based on a simple pressure mapping has been applied to axisymmetric bodies by Hoffman {17}. The partially parabolic flow assumptions have been used to solve axisymmetric flow problems by Muraoka {18} and Chen and Patel {19} and for three-dimensional flow past surface ships by Chen and Patel {19} and Muraoka {20}. An efficient streamline-iteration method with a two-equation k-ϵ turbulence model has been developed by Zhou {21} to compute turbulent flow around axisymmetric sterns.

A numerical method using a partially parabolic marching technique in a streamline coordinate system and the k-ε turbulence model has been developed by Hogan [22] to compute the turbulent flow at the stern and the wake of bodies of revolution. This method uses the modified Douglas C-S method [3,11] to provide the initial conditions at the upstream plane and the boundary conditions at a large distances outside of the boundary layer.

In this paper, the simple modification of the Douglas C-S computation method [10] will be updated and summarized. Hogan's [22] partially parabolic marching technique and the k-ε turbulence model will also be reviewed and improved. The cross-stream pressure distributions and mean velocity distributions computed by these two methods will be compared with the experimental data.

II. Simple Viscous-Inviscid Interaction Method for Axisymmetric Stern Flows

This method is an updated version of the method described in References 3 and 11. The Douglas C-S method [10] consists of using Keller's box scheme to solve the following set of partial differential equations expressing conservation of momentum and continuity.

$$u \frac{\partial u}{\partial s} + v \frac{\partial u}{\partial y} = -\frac{1}{\rho}\frac{\partial p}{\partial s} - \frac{1}{r}\frac{\partial}{\partial y}\left[r\left(\nu \frac{\partial u}{\partial y} - \overline{u'v'}\right)\right] \quad (1)$$

$$\frac{\partial}{\partial s}(ru) + \frac{\partial}{\partial y}(rv) = 0 \quad (2)$$

where u and v are the mean velocity components in the s and y directions, respectively

s,y are the coordinates parallel and normal to the body meridian, respectively,

ρ is the fluid density

p is the pressure on the body

$r = r_o(s,n) + y \cos\alpha$

r_o is the body radius

$\alpha_o = \tan^{-1}\left(\frac{dr_o}{dx}\right)$

x is the axial distance measured from the nose

ν is the kinematic viscosity of the fluid

u',v' are velocity fluctuations in the s and y directions, respectively

$\overline{u'v'}$ is the Reynolds stress

The above equations are the standard thin boundary layer equations with the addition of the transverse curvature effect, where r replaces the body radius r_o. Effects due to longitudinal curvature κ and pressure variation across the boundary layer are neglected.

The Reynolds stress $\overline{u'v'}$ is modeled by

$$-\overline{u'v'} = \nu_i \frac{\partial u}{\partial y} = \ell_i^2\left(\frac{r}{r_o}\right)\left(\frac{\partial u}{\partial y}\right)^2 \quad \text{for inner region, } 0 \le y \le y_c$$

$$-\overline{u'v'} = \nu_o \frac{\partial u}{\partial y} = \ell_o^2\left(\frac{\partial u}{\partial y}\right)^2 \quad \text{for outer region, } y_c \le y$$

$$\nu_o = 0.0168\,\gamma_{tr}\int_o^\infty (U_e-u)dy = 0.168\,U_e\delta_p^*\gamma_{tr} \quad (3)$$

$$\gamma_{tr} = \left[1 + 5.5\,(y/\delta)^6\right]^{-1}$$

= Klebanoff's intermittency factor

$$\ell_o = 0.169\left(\frac{y}{\delta}\right)\sqrt{(r_o+0.6\delta)^2-r_o^2}\,\exp\left[-\frac{6}{5}\left(\frac{y}{\delta}\right)-\frac{32}{30}\left(\frac{y}{\delta}\right)^3\right]$$

= the mixing length in the outer region of the thick boundary layer, $\delta \ge 0.23r_o$

$$\ell_i = 0.4r_o\ln\left(\frac{r}{r_o}\right)\left\{1-\exp\left[-\frac{r_o}{A}\ln\left(\frac{r}{r_o}\right)\right]\right\} \quad (4)$$

= the mixing length in the inner region of thin and thick boundary layer.

$A = 26\nu\left(\frac{\tau_w}{\rho}\right)^{-\frac{1}{2}}$, damping length

$\delta_p^* = \int_o^\delta\left(1-\frac{u}{U_e}\right)dy$, displacement thickness (planar definition)

$\delta = \delta_{995}$, boundary layer thickness where u/U_e = 0.995

U_e is the inviscid (edge) velocity used in the thin boundary layer calculations

τ_w is the wall shear stress

y_c is the value of y at which $\nu_i = \nu_o$

The flow in the wake is modeled by the following differential equation for momentum, which is simply the boundary-layer equation with skin friction neglected

$$\frac{d\Omega}{dx} + (h+2)\frac{\Omega}{U_e}\frac{dU_e}{dx} = 0 \quad (5)$$

where $\Omega = \int_o^\delta\left(1-\frac{u}{U_e}\right)\frac{u}{U_e}\,rdr$, momentum area

$\Lambda = \int_o^\delta\left(1-\frac{u}{U_e}\right)rdr$, displacement area

$h = \Lambda/\Omega$, axisymmetric shape factor

Granville [23] proposes the following equation relating h to U_e

$$h = 1 + (h_t-1)\left[\frac{\ln(U_o/U_e)}{\ln(U_o/U_t)}\right]^{1/Q} \quad (6)$$

where the subscript t denotes conditions at the tail and Q is a variable coefficient, for which Granville recommends an average value of 7.

A measure of the viscous mass-flux deficit in the thick axisymmetric boundary layer is defined by

$$U_x(r_o)\Lambda = \int_{r_o}^{r_o+\delta_r} U_x(r)\left[1-\frac{u_x(r)}{U_x(r)}\right]rdr - \int_{r_o}^{r_o+\delta_r^*} U_x(r_o)\,rdr \quad (7)$$

where r_o is the local body radius, δ_r^* the axisymmetric displacement thickness, δ_r the boundary layer thickness at which $u_x(r)/U_x(r) = 0.995$, u_x the axial viscous velocity, U_x the axial inviscid velocity, $r = r_o + y\cos\alpha_o$, and $u_x = u\cos\alpha_o - v\sin\alpha_o$. Thus the axisymmetric displacement thickness defined in equation (7) becomes

$$r_o + \delta_r^* = \sqrt{2\Delta + r_o^2} \tag{8}$$

if the variation of inviscid velocity U_x (r) across the boundary layer is assumed negligible. Following Lighthill's [8] derivation, the boundary layer displacement effect can be represented by a source distribution on the surface of the body with its source strength m of

$$2\pi r_o m = \frac{d}{dx}\left[2\pi\Delta U_x(x,r_o)\right]$$

$$\text{or} \quad m = \frac{1}{2r_o}\frac{d}{dx}\left\{\left[(r_o + \delta_r^*)^2 - r_o^2\right]U_x(x,r_o)\right\} \tag{9}$$

The equivalent blowing velocity on the body is then

$$V_N = \frac{1}{2r_o}\frac{d}{dx}\left\{\left[(r_o + \delta_r^*)^2 - r_o^2\right]U_x(x,r_o)\right\} \tag{10}$$

The boundary layer equations (1) and (2) with the modified mixing length and eddy viscosity for the outer region of a thick boundary layer [9] given in equation (3) are used to solve the mean velocity components u and v. The axial and radial velocity components are resolved by $u_x = u\cos\alpha - v\sin\alpha$ and $v_r = u\sin\alpha + v\cos\alpha$, respectively. The displacement body, the corresponding source, *and the blowing velocity are computed* according to Equations (8), (9), and (10).

The momentum area of the far wake Θ_o can be determined by equating the net rate of momentum loss of the flow to the total drag on the body. The displacement area Δ can be determined by Equations (5) and (6) in terms of the conditions of Θ_t and h_t given at the tail and Θ_o ($h=1$ at $x \to \infty$) at the far wake. In the near wake region, where neither the boundary layer equations (1) and (2) nor the simple wake model equations (5) and (6) are accurate, a fifth-degree polynomial is used [illegible] the upstream and *downstream displace-*[illegible], [illegible] the matching points X/L [illegible] 0.90 and 1.05. However, the upstream matching point must be moved upstream [illegible] separation point whenever flow separation [illegible] fairing of the displacement surface [illegible] near wake is the shortcoming of this simple [illegible] interaction procedure, which [illegible] examined in the light of a more accurate [illegible] in the next section.

[illegible] iteration process consisting of calculating pressure distributions over successive displacement bodies, or successive source or blowing velocity distributions over the original body, continues until a given difference criterion is met. Experience with the program has shown that the computed pressure coefficients for the second and third iterations usually agree to within 0.01 over most of the body. Since the results usually converge in an oscillatory manner, the final solution is taken to be the average of the values given by the last two iterations. The method of using a blowing velocity distribution is used for the final potential flow computation. The inviscid velocity components and pressure coefficients across the entire thick boundary layer are then computed.

One obvious defect of the thin boundary-layer Equations (1) and (2) is the assumption of using a constant pressure across the boundary layer for large values of y, where the velocity component parallel to the body tangent is equal to $U_o\cos\alpha_o$. However, the computed value of u approaches the inviscid velocity on the body U_e instead of $U_o\cos\alpha_o$. On the basis of a large collection of stern boundary-layer data [3,11], the inviscid influences on the computed tangential velocity u is adjusted by

$$\frac{u_m}{U_o} = \frac{u(y)}{U_e}\,\frac{U_p\cos(\alpha_o-\alpha_I)}{U_o} = f'\,\frac{U_p\cos(\alpha_o-\alpha_I)}{U_o} \tag{11}$$

where u_m is the improved tangential velocity for a thick boundary layer, $u/U_e = f'$ is the nondimentional tangential velocity predicted by the thin boundary-layer equations (1) and (2), and U_o is the free-stream velocity, $\alpha_I = \tan^{-1}[U_r(x)/U_x(x)]$, $U_p = (U_r^2+U_x^2)^{1/2}$, and U_p, U_r, U_x are the total, radial and axial inviscid velocities calculated by the final iteration of the potential-flow computation using the blowing velocity distribution. Equation (11) shows that near the body where $y \to 0$, $\alpha_I \to \alpha_o$, $U_p \to U_e$, and $u_m \to u$. At the edge of the boundary layer, where $u/U_e = f' = 1$ and

$$\frac{u_m}{U_o} = \frac{U_\delta\cos(\alpha_o-\alpha_I)}{U_o} \quad ,$$

the subscript δ denotes quantities at the edge of the boundary layer. As $y \to \infty$, $U_p \to U_o$, $\alpha_I \to 0$, and $u_m/U_o \to \cos\alpha_o$. Thus, the modified tangential velocity u_m has the proper asymptotic value $U_o\cos\alpha$ far from the body. This simple adjustment is an improvement over thin boundary layer theory where $u/U_o \to U_e/U_o$ as $y \to \infty$.

The corrected normal velocity can be obtained from the continuity *Equation* (2). The adjustment of u using formula (11) is made in the normal *y-direction and has* little effect on the variation of u in the s-direction, i.e., $\partial(ru_m)/\partial s \approx \partial(ru)/\partial s$. It follows from Equation (2) and the boundary condition that $u = u_m = v = 0$ at $y = 0$. Thus, one finds that no adjustment of the normal velocity v is required, where v is the normal velocity calculated by substituting u into Equation (2) and is much smaller than the value of u.

The axial and radial velocities u_x and v_r adjusted for the thick stern boundary layer are given by

$$\frac{u_x}{U_o} = \frac{u_m}{U_o}\cos\alpha_o - \frac{v}{U_o}\sin\alpha_o$$

$$= f'\,\frac{U_p\cos(\alpha_o-\alpha_I)}{U_o}\cos\alpha_o - \frac{v}{U_o}\sin\alpha_o \tag{12}$$

$$\frac{v_r}{U_o} = \frac{u_m}{U_o}\sin\alpha_o + \frac{v}{U_o}\cos\alpha_o$$

$$= f'\,\frac{U_p\cos(\alpha_o-\alpha_I)}{U_o}\sin\alpha_o + \frac{v}{U_e}\,\frac{U_e}{U_o} \qquad (13)$$

where $f' = u/U_e$ and v/U_e are the final solutions of the thin boundary layer Equations (1) and (2) using the average values of U_e obtained in the last two iterations of the viscous-inviscid calculation. The inviscid velocity $U = (U_x^2 + U_r^2)^{1/2}$ and the inviscid flow angle $\alpha_I = \tan^{-1}(U_r/U_x)$ are computed from the final potential-flow computation with the blowing velocity distribution, equation (10), on the original body surface, where U_r and U_x are the inviscid radial and axial velocities, respectively.

III. A Computation Procedure for the Parabolized Reynolds Equations in Axisymmetric Flow Using Streamline Coordinates and the k-ε Turbulence Model

The natural coordinate system shown in Fig. 1 is one in which one coordinate s lies along the streamline and the other two n,θ are normal to the streamline (Liepmann and Roshko [24]). For axisymmetric flow, $\partial/\partial\theta = 0$ where $\partial/\partial\theta = 0$ θ is in the azimuthal direction for axisymmetric flow. In the Reynolds-average Navier-Stokes equations, the diffusion terms along the mean streamline direction are usually very small and are neglected, the Reynolds equations with such an approximation are

$$U\frac{\partial U}{\partial s} = -\frac{1}{\rho}\frac{\partial p}{\partial s} + \frac{1}{r}\frac{\partial}{\partial n}\left[\nu_e r\frac{\partial U}{\partial n}\right] \qquad (14)$$

$$\nu_e = \nu + \nu_T$$

and $$U^2\frac{\partial\alpha}{\partial s} = -\frac{1}{\rho}\frac{\partial p}{\partial n} \qquad (15)$$

where U is the total mean velocity along the streamline direction s, n is the distance normal to the mean streamlines, r is the radial distance from the body axis x, p is the mean pressure, α is the angle of the streamline with the x-axis, $\nu_e = \nu + \nu_T$, ν is the molecular kinematic viscosity, and ν_T is the turbulent eddy viscosity. A stream function ψ is defined for axisymmetric flow

$$d\psi = rU\,dn \qquad (16)$$

As shown in Fig. 1, the transformation of the equations to the (x, ψ) coordinate system can be obtained with the aid of the following relationships

$$\frac{\partial()}{\partial s} = \frac{\partial()}{\partial x}\frac{\partial x}{\partial s} + \frac{\partial()}{\partial\psi}\frac{\partial\psi}{\partial s} = \cos\alpha\frac{\partial()}{\partial x} \qquad (17)$$

and $$\frac{\partial()}{\partial n} = \frac{\partial()}{\partial x}\frac{\partial x}{\partial n} + \frac{\partial()}{\partial\psi}\frac{\partial\psi}{\partial n} = rU\frac{\partial()}{\partial\psi} - \sin\alpha\frac{\partial()}{\partial x} \qquad (18)$$

where $\frac{dx}{dn} = -\sin\alpha$, $\frac{dx}{ds} = \cos\alpha$, $\frac{dr}{dn} = \cos\alpha$, $\frac{dr}{ds} = \sin\alpha$

$$-\frac{d\alpha}{ds} = \frac{1}{R} = \kappa \text{ and } d\psi = rU\,dn = rU(\cos\alpha\,dr - \sin\alpha\,dr)$$

The transformed Equations (14) and (15) in the (x, ψ) coordinate system are

$$U\cos\alpha\frac{\partial U}{\partial x} = -\cos\alpha\frac{\partial}{\partial x}\left[\frac{p}{\rho}\right] + \frac{\sin\alpha}{r}\frac{\partial}{\partial x}\left[r\,\nu_e\sin\alpha\frac{\partial U}{\partial x}\right]$$

$$-\frac{\sin\alpha}{r}\frac{\partial}{\partial x}\left[r^2\nu_e U\frac{\partial U}{\partial\psi}\right] - U\frac{\partial}{\partial\psi}\left[r\nu_e\sin\alpha\frac{\partial U}{\partial x}\right]$$

$$+U\frac{\partial}{\partial\psi}\left[r^2\nu_e U\frac{\partial U}{\partial\psi}\right] \quad \text{and} \qquad (19)$$

$$U^2\cos\alpha\frac{\partial\alpha}{\partial x} = \sin\alpha\frac{\partial}{\partial x}\left[\frac{p}{\rho}\right] - rU\frac{\partial}{\partial\psi}\left[\frac{p}{\rho}\right] \equiv -\frac{1}{\rho}\frac{\partial p}{\partial n} \qquad (20)$$

The turbulent eddy viscosity ν_T in Equation (19) is modeled by the two k-ε equations governing the interaction of the turbulence with the mean flow. The turbulence kinetic energy is defined as $k = \Sigma\overline{u_i'^2}/2$, and the turbulence energy dissipation is defined as $\varepsilon = \nu\overline{(\partial u_i/\partial x_m)(\partial u_i/\partial x_m)}$. It is assumed that the eddy viscosity is determined by dimensional analysis as

$$\nu_T = \frac{C_\mu k^2}{\varepsilon} \qquad (21)$$

The k-ε equations developed by Hanjalic and Launder [25] can be written in the (s,n) coordinate system as

$$U\frac{\partial k}{\partial s} = \frac{1}{r}\frac{\partial}{\partial n}\left(\frac{\nu_T}{\sigma_k}r\frac{\partial k}{\partial n}\right) + \nu_T\left(\frac{\partial U}{\partial n}\right)^2 - \frac{1}{3}k\frac{\partial U}{\partial s} - \varepsilon \qquad (22)$$

and

$$U\frac{\partial\varepsilon}{\partial s} = \frac{1}{r}\frac{\partial}{\partial n}\left(\frac{\nu_T}{\sigma_\varepsilon}r\frac{\partial\varepsilon}{\partial n}\right) + C_1\frac{\varepsilon}{k}\nu_T\left(\frac{\partial U}{\partial n}\right)^2 - C_3\varepsilon\frac{\partial U}{\partial s}$$

$$-C_2\frac{\varepsilon^2}{k} \qquad (23)$$

All the turbulence diffusion terms in Equations (22) and (23) have been neglected except the term $(\overline{u'^2} - \overline{v'^2})\partial u/\partial s \cong (k/3)\partial u/\partial s$ in the turbulence production. Hanjalic and Launder [25] recommend the retention of this term to emphasize the role of irrotational deformations in promoting energy transfer. The constants C_μ, C_1, C_2, C_3, σ_k and σ_ε as given by Hanjalic and Launder [25] are 0.09, 1.44, 1.90, 4.44, 1.0, and 1.30, respectively. The transformation of the k-ε equations (22) and (23) into the (x,ψ) coordinate system has been made by Hogan [22] using equations (16), (17), and (18), e.g.

$$U \cos\alpha \frac{\partial k}{\partial x} = \frac{\sin\alpha}{r}\frac{\partial}{\partial x}\left[\frac{r\nu_e}{\sigma_k}\sin\alpha\frac{\partial k}{\partial x}\right] - \frac{\sin\alpha}{r}\frac{\partial}{\partial x}\left[\frac{r^2\nu_e}{\sigma_k}U\frac{\partial k}{\partial \psi}\right] - U\frac{\partial}{\partial \psi}\left[\frac{r\nu_e}{\sigma_k}\sin\alpha\frac{\partial k}{\partial x}\right] + U\frac{\partial}{\partial \psi}\left[\frac{r^2\nu_e}{\sigma_k}U\frac{\partial k}{\partial \psi}\right] + \nu_T\left[rU\frac{\partial U}{\partial \psi} - \sin\alpha\frac{\partial U}{\partial x}\right]^2 - 1/3\, k\cos\alpha\frac{\partial U}{\partial x} - \varepsilon \tag{24}$$

$$U \cos\alpha \frac{\partial \varepsilon}{\partial x} = \frac{\sin\alpha}{r}\frac{\partial}{\partial x}\left[\frac{r\nu_e}{\sigma_\varepsilon}\sin\alpha\frac{\partial \varepsilon}{\partial x}\right] - \frac{\sin\alpha}{r}\frac{\partial}{\partial x}\left[\frac{r^2\nu_e}{\sigma_\varepsilon}U\frac{\partial \varepsilon}{\partial \psi}\right] - U\frac{\partial}{\partial \psi}\left[\frac{r\nu_e}{\sigma_\varepsilon}\sin\alpha\frac{\partial \varepsilon}{\partial x}\right] + U\frac{\partial}{\partial \psi}\left[\frac{r^2\nu_e}{\sigma_\varepsilon}U\frac{\partial \varepsilon}{\partial \psi}\right] + C_1\frac{\varepsilon}{k}\nu_T\left[rU\frac{\partial U}{\partial \psi} - \sin\alpha\frac{\partial U}{\partial x}\right]^2 - 1/3\, C_1\varepsilon\cos\alpha\frac{\partial U}{\partial x} - C_2\frac{\varepsilon^2}{k} \tag{25}$$

[illegible] computation procedure starts at a sta- [illegible] the body where the boundary layer is thin [illegible] downstream into the wake. As shown [illegible] the boundary conditions for the values [illegible] equations (19) and (20) over the [illegible] and along a cylindrical stream [illegible] the boundary layer/wake are [illegible] values obtained from the [illegible] interaction computations [illegible] II. The stream surface ψ_T is [illegible] that it lies entirely outside the [illegible] boundary layer and wake of the flow [illegible] the values of k and [illegible] in [illegible] and (25) are zero. Furthermore, [illegible] dissipation is assumed to [illegible] production inside the thin [illegible] of the inlet plane, e.g., [illegible] $= -\overline{u'v'}$ [illegible], the distributions of [illegible] and k [illegible] boundary layer can be estimated by

$$[illegible] \tag{26}$$

$$[illegible] \tag{27}$$

where the values of ℓ, ν_T, and $\partial u/\partial y$ are obtained from the final iteration of the simple viscous-inviscid interaction computations. The lower boundary in the computation domain is the stream surface ψ_o which lies along the body's surface and along r=0 in the wake. The boundary conditions on ψ=0 in the wake are r=α=0, and $\partial U/\partial\psi = \partial p/\partial\psi = \partial k/\partial\psi = \partial\varepsilon/\partial k = 0$. The boundary conditions on the body (ψ_o at ψ=0) are $r = r_o$, U=0, $\alpha = \alpha_o = \tan^{-1}(dr_o/dx)$, and the condition for pressure provided by equation (20)

$$\rho U^2 \cos\alpha \frac{\partial \alpha}{\partial x} = 0 = -\frac{\partial p}{\partial n} = \sin\alpha_o\frac{\partial p}{\partial x} - rU\frac{\partial p}{\partial n}$$

Again, the assumption of $\varepsilon = -\overline{u'v'}\,\partial U/\partial n$ is used to obtain the boundary conditions for ε and k as estimated by equations (26) and (27) on the body (ψ = 0). However, the values of ε and k are not taken at the wall but at a small distance from the wall (usually $nu_*/\nu \simeq 50$) where the inner region of the mixing length and eddy viscosity

$$\ell_i = 0.4\, r_o \ln\left(\frac{r}{r_o}\right)\left\{1 - \exp\left[-\frac{r_o}{A}\ln\left(\frac{r}{r_o}\right)\right]\right\}$$

and (28)

$$\nu_T = \ell_i^2\left(\frac{r}{r_o}\right)\frac{\partial U}{\partial n}$$

is valid.

An iterative numerical marching procedure has been developed by Hogan [22] to solve equations (19), (20), (24), and (25) within the partially parabolic flow assumption that the inconsistent pressure field downstream is communicated to the upstream. The overall numerical procedure of Hogan [22] is used here; however, the numerical details for solving the k-ε equations (24) and (25) have been improved in this paper.

IV. Numerical Results

Using the numerical procedure developed in Sections II and III, calculations were performed for four bodies for which experimental data were available. These are designated as DTNSRDC axisymmetric Model 1 (Huang et al. [3]), DTNSRDC axisymmetric Model 5 (Huang et al. [4]), Model A, and Model B (Lyon [26,27]). Table 1 lists the following geometric and flow parameters for each body: the length of the body L, the maximum radius of the body r_{max}, the upstream flow velocity U_o, and the body Reynolds number R_L. No flow separation on the four models was measured or predicted. The measured and computed mean flow characteristics over the sterns of the four models are shown in Figures 2 through 5. In all cases, the wall functions used in the k-ε turbulence model are taken as the values of k and ε computed from equations (26), (27) and (28) with nu_*/ν set equal to 50. The simple viscous-inviscid interaction computation is the computation procedure outlined in Section II and the method designated as the "parabolized N.-S. calculation" is the numerical procedure of solving the parabolized Reynolds-averaged Navier-Stokes equations using streamline coordinates and the k-ε turbulence model summarized in Section III.

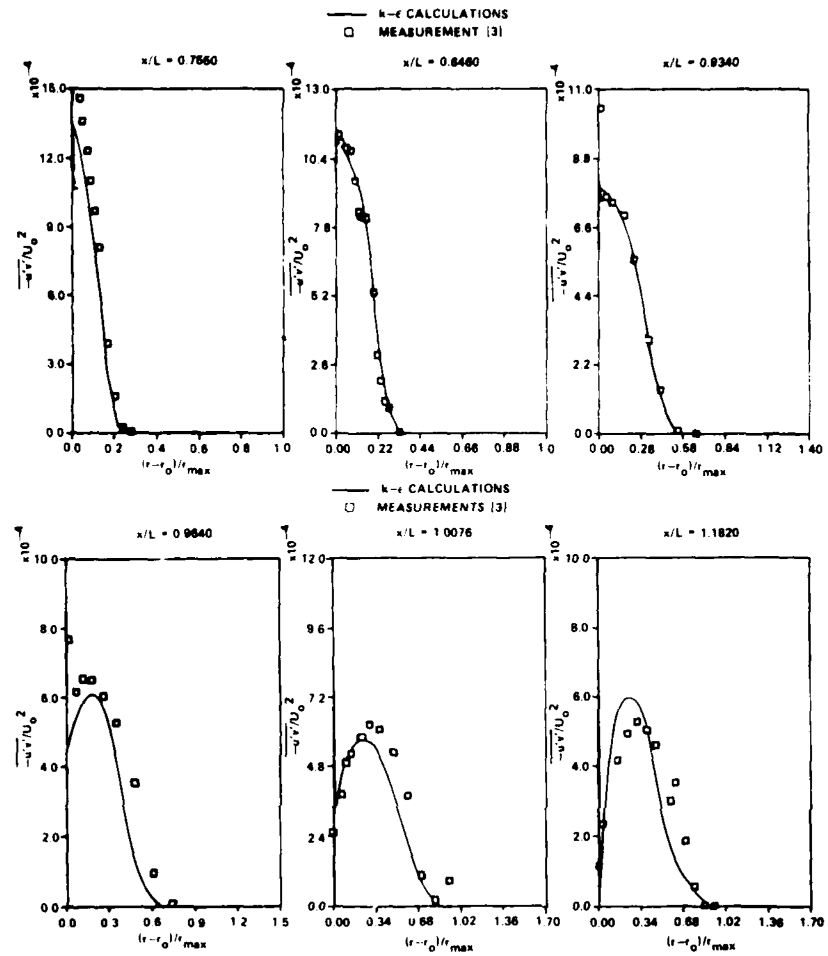

(a) DTNSRDC Axisymmetric Model 1

Figure 7 - The Normal Reynolds Stress Profiles Across Thick Stern Boundary Layers

Figure 6 - (Continued)

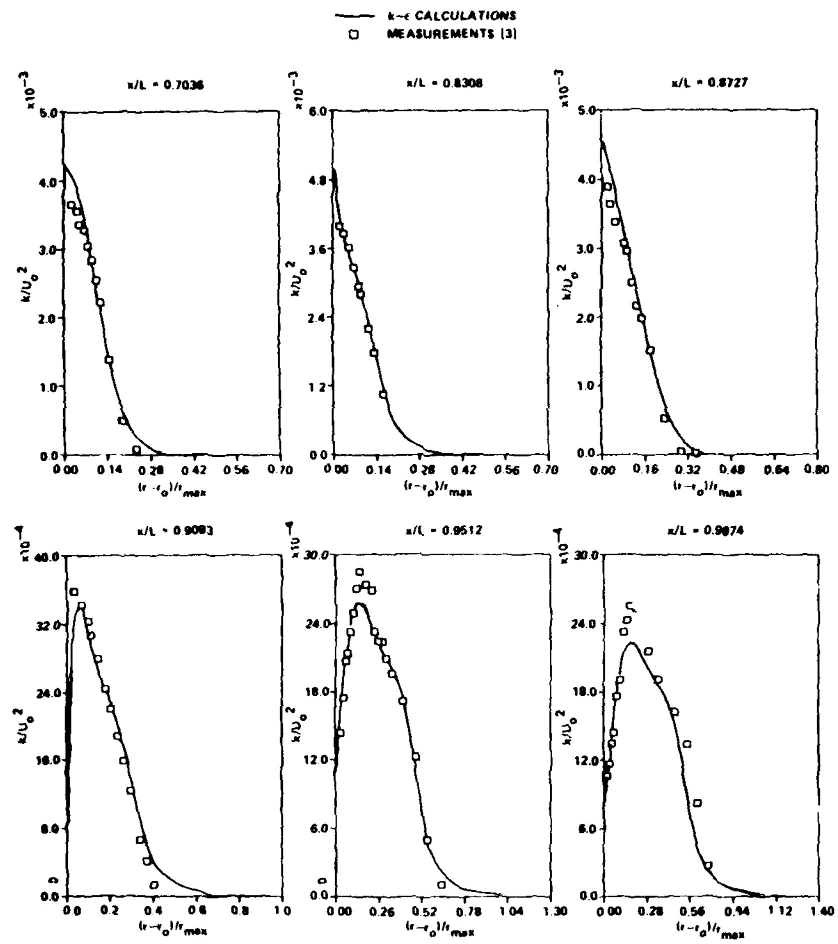

(b) DTNSRDC Axisymmetric Model 5

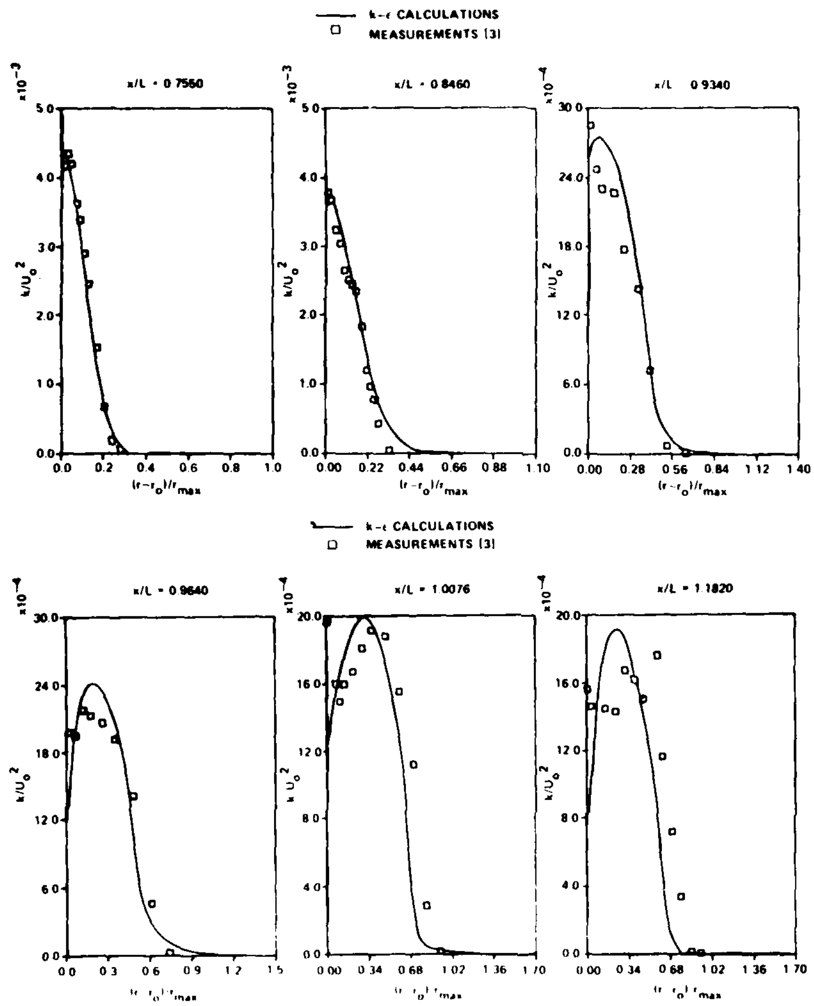

(a) DTNSRDC Axisymmetric Model I

Figure 6 - The Turbulent Kinetic Energy Profiles Across Thick Stern Boundary Layers

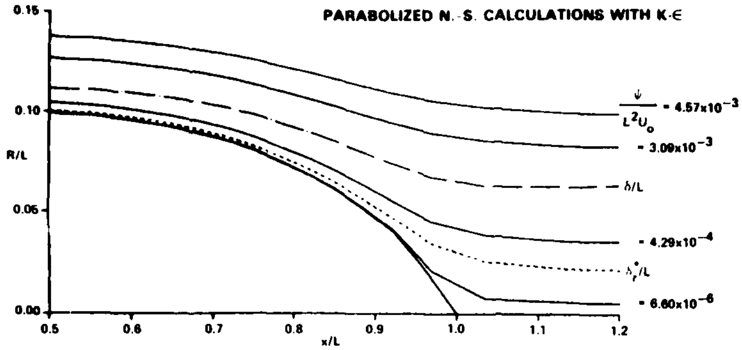

(a) Stream Surfaces and Boundary Layer Thicknesses

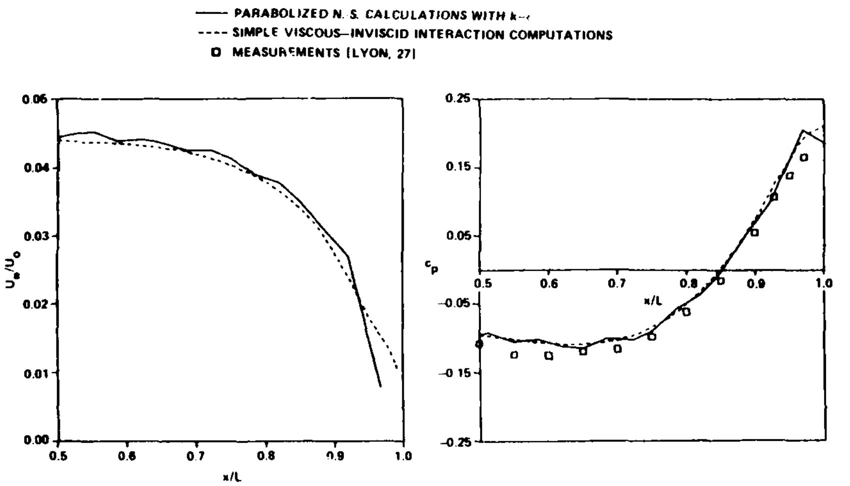

(b) Distribution of Nondimensional Frictional Velocity

(c) Distribution of Pressure Coefficient on the Stern

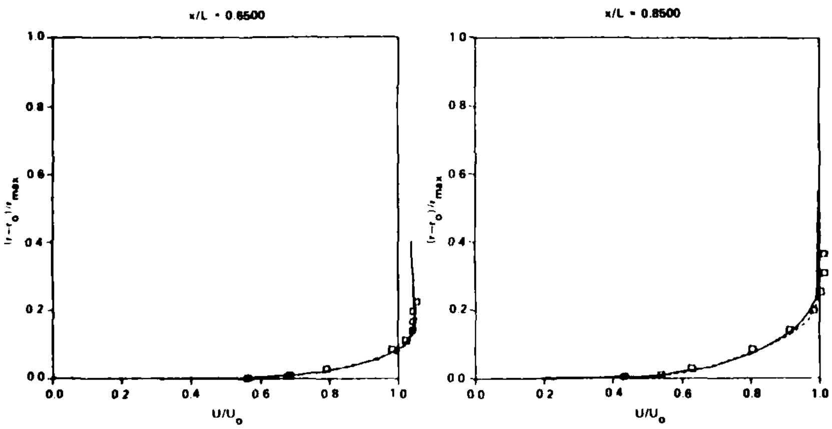

(d) Mean Total Velocity Profiles

Figure 5 - Comparison of the Measured and Computed Mean Flow Characteristics Over the Stern of Lyon Model B

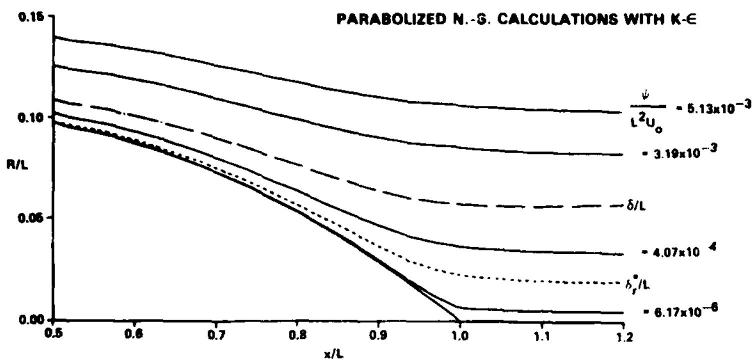

(a) Stream Surfaces and Boundary Layer Thicknesses

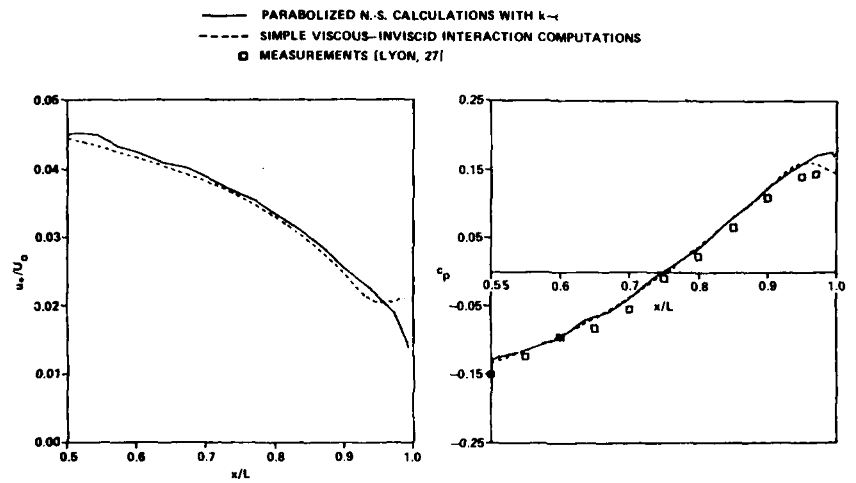

(b) Distribution of Nondimensional Frictional Velocity

(c) Distribution of Pressure Coefficient on the Stern

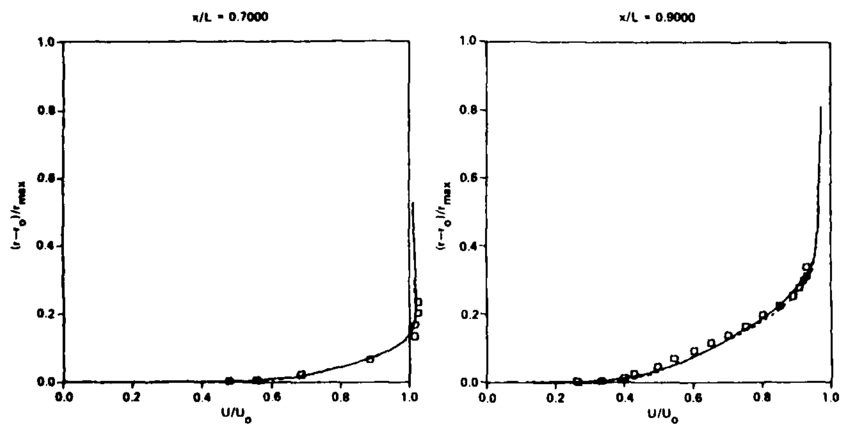

(d) Mean Total Velocity Profiles

Figure 4 - Comparison of the Measured and Computed Mean Flow Characteristics Over the Stern of Lyon Model A

Figure 3 - (Continued)

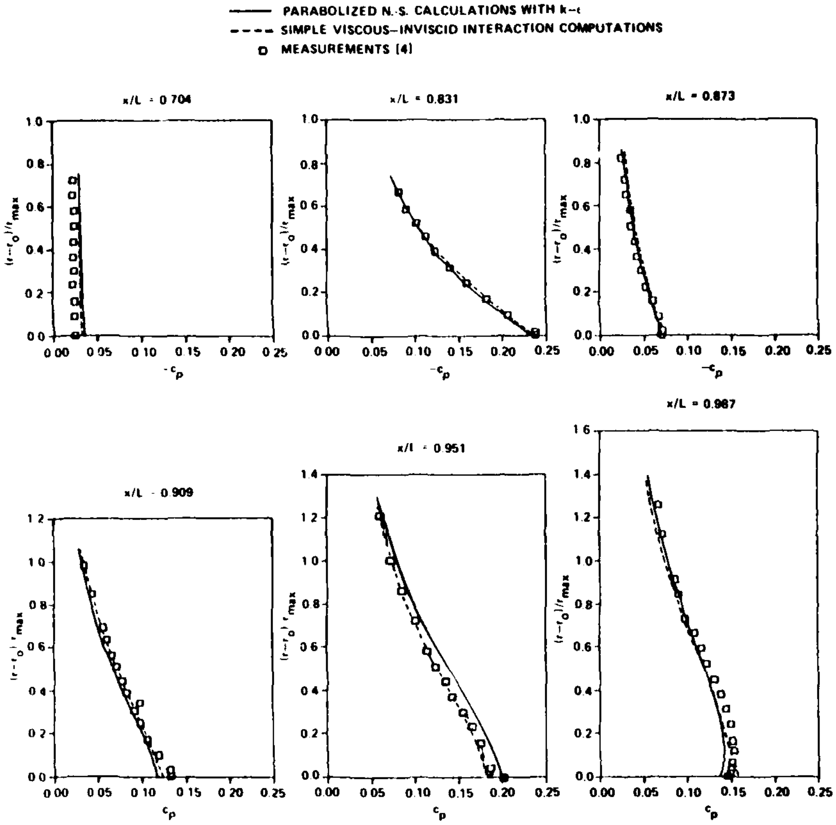

(e) Distributions of Pressure Coefficients

Figure 3 - (Continued)

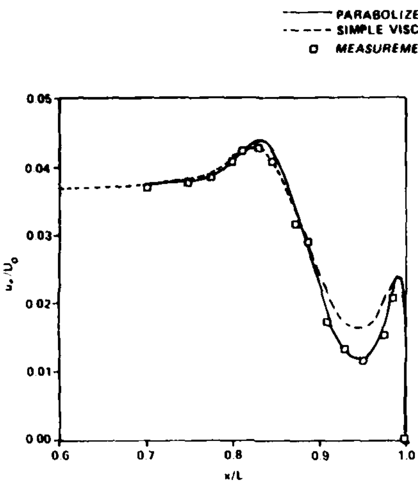

(b) Distribution of Nondimensional *Frictional Velocity*

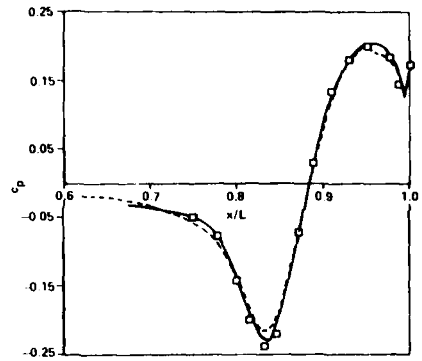

(c) Distribution of Pressure Coefficient on the Stern

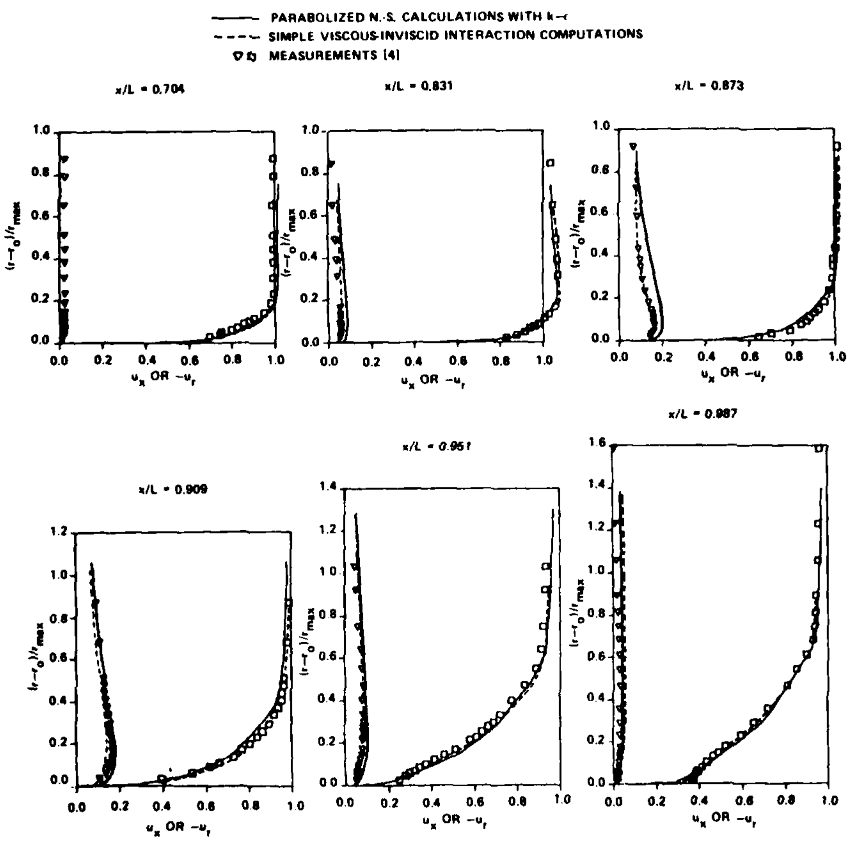

(d) Mean Axial and Radial Velocity Profiles

Figure 2 - (Continued)

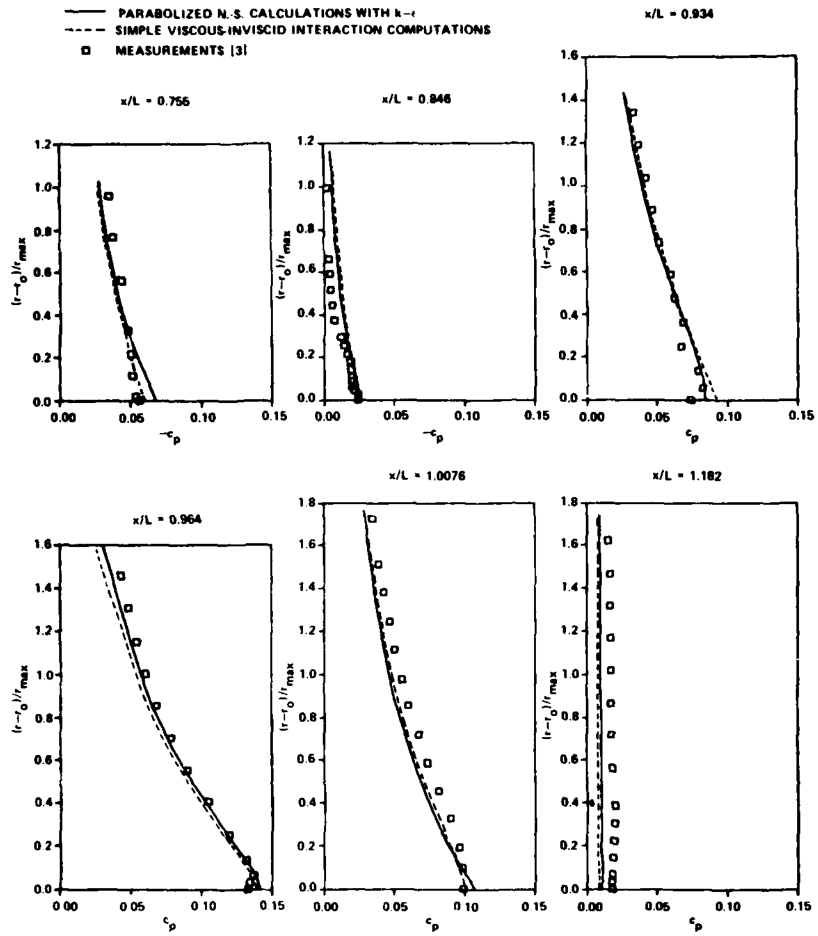

(e) Distributions of Pressure Coefficients

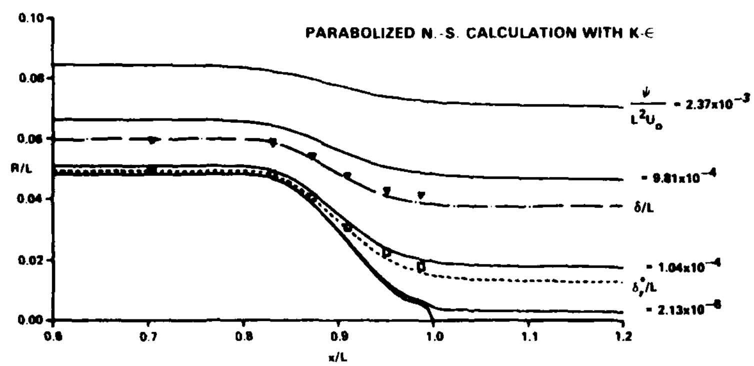

(a) Stream Surfaces and Boundary Layer Thicknesses

Figure 3 - Comparison of the Measured and Computed Mean Flow Characteristics Over the Stern of DTNSRDC Axisymmetric Model 5

Figure 2 - (Continued)

——— PARABOLIZED N.S. CALCULATIONS WITH k-ε
- - - - SIMPLE VISCOUS-INVISCID INTERACTION COMPUTATIONS
□ MEASUREMENTS [3]

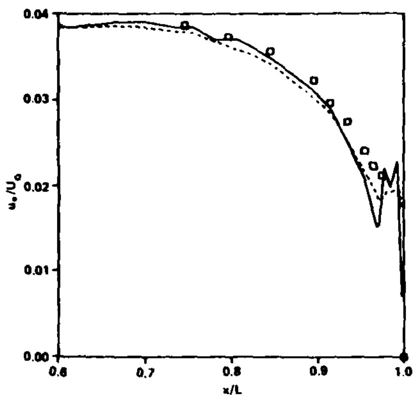

(b) Distribution of Nondimensional Frictional Velocity

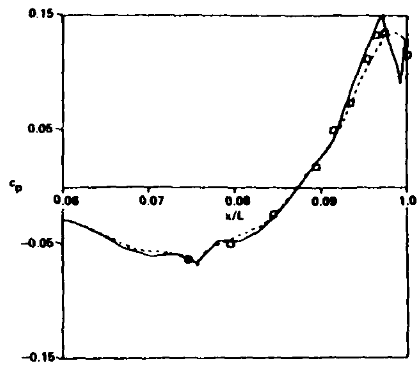

(c) Distribution of Pressure Coefficient on the Stern

——— PARABOLIZED N.S. CALCULATIONS WITH k-ε
- - - - SIMPLE VISCOUS-INVISCID INTERACTION COMPUTATIONS
▽ □ MEASUREMENTS [3]

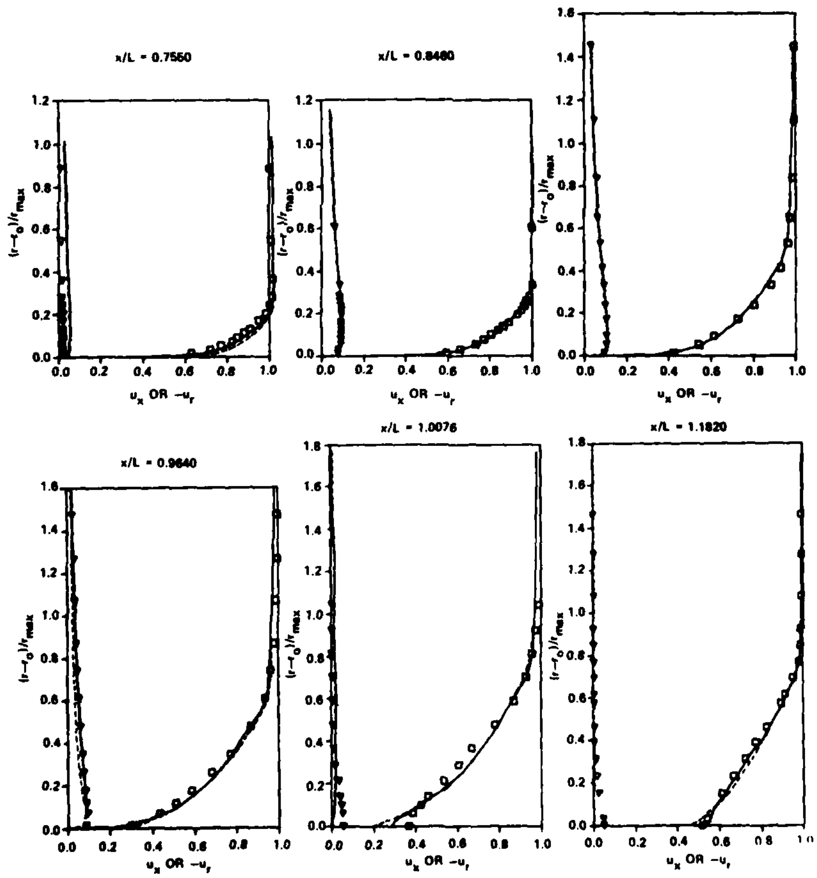

(d) Mean Axial and Radial Velocity Profiles

τ_w Wall shear stress

ψ Stream function

ψ_T Outer streamline grid number

Ω Momentum area defined in equation 5

Ω_0 Momentum area of the far wake

Subscripts

e Value of inviscid velocity used for thin boundary-layer/wake computation

r Radial direction

t Value at trailing edge of the body

x Axial direction

δ Value at the outer edge of the boundary layer

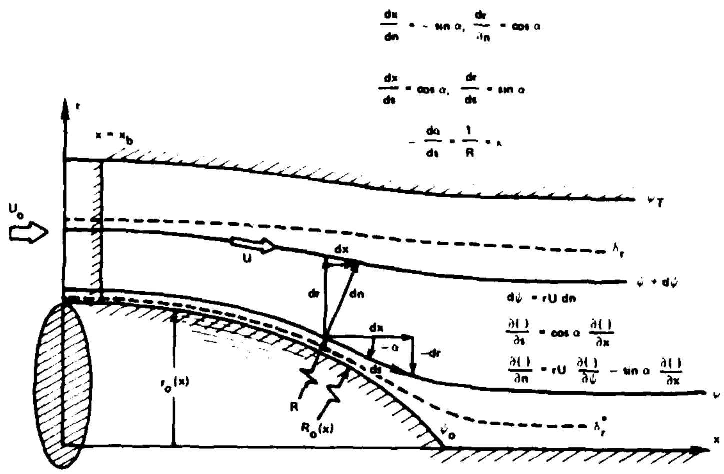

Figure 1 - Natural Coordinate System and Notation.

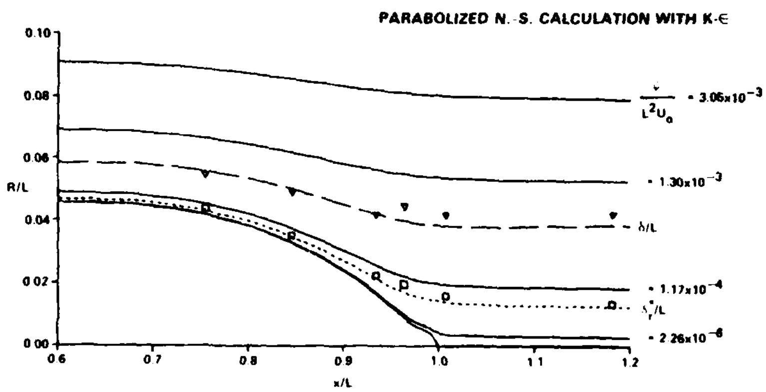

(a) Stream Surfaces and Boundary Layer Thicknesses

Figure 2 - Comparison of the Measured and Computed Mean Flow Characteristics Over the Stern of DTNSRDC Axisymmetric Model 1

NOTATION

c_p Coefficient of pressure $= \dfrac{p - p_o}{1/2\rho U_o^2}$

C_1 Numerical constant in the k-ε model = 1.44

C_2 Numerical constant in the k-ε model = 1.90

C_3 Numerical constant in the k-ε model = 4.44

$C_D = C_\mu$ Numerical constant is the k-ε model = 0.09

k Turbulent kinetic energy

L Length of the body

ℓ Mixing length

ℓ_i Mixing length in the inner region of boundary layer defined in equation (4)

ℓ_o Mixing length in the outer region of boundary layer defined in equation (4)

n Distance measured normal to the mean streamlines

p Mean pressure

p_o Upstream pressure

R Radius of curvature of a streamline

R_e Reynolds number of the flow $= U_oL/\nu$

r Radial distance measured from body axis

r_{max} Maximum radius of the body

r_o Body radius

s Distance measured along a streamline or body meridian

U Total mean velocity along the streamline direction

U_e Inviscid (edge) velocity used for thin boundary layer computation

U_o Free-stream velocity

U_p Total inviscid velocity $= (U^2_x + U^2_r)^{1/2}$

U_r Inviscid radial velocity

U_x Inviscid axial velocity

u Mean velocity component parallel to the body meridian

u' Turbulent velocity in the s-direction

u_m Modified value of u defined in equation (11)

u_x Mean axial velocity

u_* Friction velocity $= (\tau_w/\rho)^{1/2}$

v Mean velocity component normal to the body meridian

v' Turbulent velocity in the y- or n-direction

v_r Mean radial velocity

w' Turbulent velocity in the θ direction

x Coordinate measured along the axis of the body measured from the nose

x_b Beginning x-station of the partially parabolic k-ε calculations

y Distance measured from the body surface normal to the body meridian

y_c Value of y at which $\nu_i = \nu_o$ or $\ell_i = \ell_o$

α Angle of streamline with the x-axis

α_I Angle of inviscid streamline with the x-axis

α_o Angle of body surface with the x-axis, $\alpha_o = \tan^{-1}(dr_o/dx)$

γ_{tr} Klebanoff's intermittency factor defined in equation (3)

$\delta = \delta_{995}$ Boundary layer thickness = position where the velocity is 99.5% of the potential flow velocity

δ_r Radial distance of boundary layer thickness, $\delta_r = \delta\cos\alpha_o$.

δ_r^* Axisymmetric displacement thickness defined in equation (8)

ε Turbulent kinetic energy dissipation

θ Azimuthal angle

κ Longitudinal curvature

Λ Displacement area defined in equation (7)

ν Molecular kinematic viscosity of the fluid

ν_e Total effective viscosity $= \nu + \nu_T$

ν_i Inner eddy vicosity defined in equation (3)

ν_o Outer eddy viscosity defined in equation (3)

ν_T Turbulent eddy viscosity

ρ Constant fluid density

σ_k Turbulent Prandtl number used in the k equation = 1.0

σ_ε Turbulent Prandtl number used in the ε equation = 1.30

[7] Huang, T.T., N.C. Groves, and G.S. Belt, "Stern Boundary-Layer Flow on Two Three Dimensional Bodies Having Elliptical Transverse Cross Sections," Presented at Second Symposium on Numerical and Physical Aspects of Aerodynamic Flows, California State University, Long Beach, California (17-20 Jan 1983).

[8] Lighthill, M.J., "On Displacement Thickness," J. of Fluid Mechanics, 4, pp. 383-392 (1958).

[9] Huang, T.T., "Measured Similarity Properties of Eddy Viscosity and Mixing Length in Three-Dimensional Turbulent Stern Flows," paper to be presented at Second International Symposium on Ship Viscous Resistance, Göteborg, Sweden (March 18-20, 1985).

[10] Cebeci, T. and Smith, A.M.O., Analysis of Turbulent Boundary Layers, Academic Press, Inc., New York, N.Y., 1974, pp. 258-297.

[11] Wang, H.T. and T.T. Huang, "Calculation of Potential Flow/Boundary Layer Interaction on Axisymmetric Bodies," paper presented at the Joint ASME-CSME Turbulent Boundary Layers Conference, Niagara Falls, N.Y. (18-20 Jun 1979).

[12] Nakayama, A., Patel, V.C., and Landweber, L., "Flow Interaction Near the Tail of a Body of Revolution, Part 1: Flow Exterior to Boundary Layer and Wake," ASME Journal of Fluids Engineering, Vol. 98, pp. 531-537 (Sept 1976).

[13] Nakayama, A., Patel, V.C., and Landweber, L., "Flow Interaction Near the Tail of a Body of Revolution, Part 2: Iterative Solution for Flow Within and Exterior to Boundary Layer and Wake," ASME Journal of Fluids Engineering, Vol. 98, pp. 538-549 (Sept 1976).

[14] Dyne, G., "A Streamline Curvature Method for Calculating the Viscous Flow Around Bodies of Revolution," Paper No. 6, International Symposium on Ship Viscous Resistance, Göteborg, Sweden (Aug-Sep 1978).

[15] Head, M.R., "Entrainment in the Turbulent Boundary Layer," Reports and Memoranda No. 3152, Aeronautical Research Committee, London, England (Nov. 1960).

[16] Lee, Yu-Tai, "Thick Axisymmetric Turbulent Boundary Layer and Wake of a Low-Drag Body," Ph.D. Thesis, The University of Iowa (Dec. 1978).

[17] Hoffman, G.H., "A Modified Displacement-Body Method for Treating the Axisymmetric Strong-Interaction Problem," J. of Ship Research, Vol. 24, No. 2, pp. 114-122 (June 1980).

[18] Muraoka, K., "Calculation of Thick Boundary Layer and Wake of Ships by a Partially Parabolic Method," 13th Symposium on Naval Hydrodynamics, Tokyo, Japan, pp. 601-614 (1980).

[19] Chen, H.C., and V.C. Patel, "Calculation of Stern Flows by Time Marching Solution of the Partially-Parabolic Equations," Proceedings of 15th Symposium on Naval Hydrodynamics, Hamburg, Federal Republic of Germany, (Sept 1984).

[20] Muraoka, K., "Calculation of Viscous Flow Around Ship Stern," Transactions of the West-Japan Society of Naval Architects, 58, pp. 235-257 (1978).

[21] Zhou, L.D., "A Streamline-Iteraction Method for Calculating Turbulent Flow Around the Stern of a Body of Revolution and Its Wake," 14th Symposium on Naval Hydrodynamics, Ann Arbor, Michigan (1982). Proceedings published by National Academy Press, Wash., D.C., pp. 1041-1069 (1983).

[22] Hogan, T.F., "A Calculation of the Parabolized Navier-Stokes Equations for Turbulent Axisymmetric Flows Using Streamline Coordinates and the k-ε Turbulence Model," Report DTNSRDC-83/070 (Nov. 1983).

[23] Granville, P.S., "The Calculation of the Viscous Drag of Bodies of Revolution," Report 849, July 1953, David Taylor Model Basin, Bethesda, MD.

[24] Liepmann, H.W. and A. Roshko, Elements of Gasdynamics, John Wiley and Sons, Inc., New York (1957).

[25] Hanjalic, K. and B.E. Launder, "Sensitizing the Dissipation Equation to Irrotational Strains," Journal of Fluids Engineering, 102, pp. 34-40 (1980).

[26] Lyon, H.M., "The Effect of Turbulence on the Drag of Airship Models," Report and Memoranda No. 1511, Aeronautical Research Committee, London, England, pp. 123-148 (1932).

[27] Lyon, H.M., "A Study of the Flow in the Boundary Layer of Streamline Bodies," Report and Memoranda No. 1622, Aeronautical Research Committee, London, England, pp. 266-318 (1934).

Extensive measurements of the pressure field were made for the flows past Models 1 and 5 (Huang et al. [3,4]. Comparisons of the computed with the experimental pressure fields for the two bodies are given in Figures 2e through 3e. The computed pressure profiles and the experimental pressure fields for Model 1 (Figure 2e) are within 1.5%; for Model 5 (Figure 3e) the results differ by 2%. The computed pressure profiles agree very well with the experimental results above the boundary-layer region.

The differences between the computed pressure coefficients by the two methods are all less than 1% outside the displacement surface and less than 2% near the body. This indicates that the simple viscous-inviscid interaction computation procedure using the displacement body concept and the revised mixing length correctly determined the essential features of the thick stern boundary layer. Only near the very tail end of the body, the parabolized N.-S. calculations are found to model the flow better than the simple interaction procedure (Fig. 3b and 3c). Chen and Patel [19] have also obtained very good results in the tail region of the Model 5, by their parabolized method.

The results of the turbulent kinetic energy calculations for Model 1 and Model 5, together with experimental results, are given in Figure 6. The agreement of the computed k with the experimental data is good. These results are encouraging and indicate that the use of the inner mixing length with the k-ε model gives a good approximation to the turbulent field. In the wake, the agreement is satisfactory.

The measured and computed Reynolds stress profiles, $\overline{-u'v'}$, are presented for Model 1 and Model 5 in Figure 7. The agreement of the computed results and the experimental data is also satisfactory for model 1. The measured values of $\overline{-u'v'}$ for model 5 are higher than the predicted values at $X/L > 0.87$.

Overall, the agreement between the measured and calculated results is encouraging. For most of the flow field, the velocity, and the pressure profiles are correctly predicted by the two methods. The wall pressure and shear stress distributions computed by the two methods also agree well with the experimental data. The measured distributions of turbulence kinetic energy k and Reynolds stress are satisfactorily predicted by the k-ε turbulence model used.

V. Conclusion

Two viscous-inviscid interaction computation procedures are presented. One method solves the parabolized Reynolds-averaged Navier-Stokes equations using streamline coordinates and the k-ε turbulence model and the other method solves the simpler thin boundary layer equations using the Lighthill displacement body concept and the revised mixing length for the thick boundary layer. The tangential velocities computed by the thin boundary layer equations are adjusted to account for the inviscid influence in the simple method. The maximum difference in the computed axial and radial velocities between the two methods is about two percent of the free-stream velocity and the maximum difference in the computed cross-stream pressure coefficients is less than one percent outside the displacement surface and is about two percent near the body. Only near the very tail end of the body are the parabolized Navier-Stokes calculations found to model the flow better than the simple method. The prediction of surface pressure coefficients and friction velocities, normalized axial and radial velocities and cross-stream pressure coefficients are in close agreement with the experimental data for four models having attached flows. Except for the surface friction velocities near the tail end of the body, an overall agreement of the above quantities by the two computation methods has been obtained. The developed simple and efficient viscous-inviscid interaction computation procedure can be used as a design tool to compute the cross-stream velocity and pressure variation across the thick stern boundary layer for many practical naval applications.

Acknowledgement

The initial phase of this paper was funded under the David W. Taylor Naval Ship Research and Development Center's Independent Research Program, Program Element 61152N, Task Area ZR0230101 and DTNSRDC Work Units 1542-103(FY84), 1542-140.

The authors would like to thank Mrs. Nancy Groves for her assistance in the preparation of this paper, which was supported by the General Hydrodynamics Research Program, Program Element 61153N, Task Area SR0230101, DTNSRDC Work Unit 1542-070.

References

[1] Huang, T.T., H.T. Wang, N. Santelli, and N.C. Groves, "Propeller/Stern/Boundary-Layer Interaction on Axisymmetric Bodies: Theory and Experiment," DTNSRDC Report DTNSRDC76-00113 (Dec 1976).

[2] Huang, T.T. and B. Cox, "Interaction of Afterbody Boundary Layer and Propeller," Symposium on Hydrodynamics of Ship and Offshore Propulsion System, Hovik outside Oslo, Norway (Sponsor Det Norske Veritas) (20-25 Mar 1977).

[3] Huang, T.T., N. Santelli, and G.S. Belt, "Stern-Boundary-Layer Flow on Axisymmetric Bodies," Presented at the 12th Symposium on Naval Hydrodynamics, Washington, D.C., (5-9 Jun 1978). Available from National Academy of Sciences, Wash., D.C., pp. 127-147 (1979).

[4] Huang, T.T., N. Groves, and G. Belt, "Boundary-Layer Flow on an Axisymmetric Body with an Inflected Stern," DTNSRDC 80/064, (Jul 1980).

[5] Groves, N.C., G.S. Belt, and T.T. Huang, "Stern Boundary-Layer Flow on a Three-Dimensional Body of 3:1 Elliptical Cross-Section," Report DTNSRDC-82/022 (May 1982).

[6] Huang, T.T., N.C. Groves, and G.S. Belt, "Stern Boundary-Layer Flow on a Three Dimensional Body of 2:1 Elliptical Cross-Section," Report DTNSRDC-84/022 (Oct 1984).

TABLE 1 - FLOW AND BODY GEOMETRY PARAMETERS

	L (m)	r_{max} (m)	U_∞ (m/s)	R_e
Model 1	3.066	0.1398	30.48	6.60×10^6
Model 5	2.910	0.1398	45.72	9.30×10^6
Model A	1.778	0.1778	17.88	2.09×10^6
Model B	1.778	0.1778	17.88	2.05×10^6

The numerical results display a thickening of the turbulent region in the stern/wake regions of the flows. The displacement bodies diverge significantly from the physical bodies near the stern and continue into the wake with slowly decreasing radii. In Figures 2a and 3a, the computed displacement body and boundary layer thickness are compared to the values of δ^* and δ obtained from the data of Huang et al. [3,4]. For both bodies, the computed δ^* and δ lie slightly below the experimental results in the stern/wake region, but, overall, the agreement with the experiments is good.

The distributions of the frictional velocity u_* are shown in Figures 2b, 3b, 4b and 5b and the wall-pressure coefficient c_p are shown in Figures 2c, 3c, 4c, and 5c for the four bodies. The pressure distribution computed by the parabolic N.-S. method for Model 1 (Figure 2c) has a large trough at the inflected stern. In this region of the body, the surface and the streamlines near the surface have a marked change in curvature. As the streamlines change curvature from convex to concave, the pressure gradient changes from adverse to favorable. Following the concave part of the stern, the streamline curvature becomes convex again, with a corresponding rise in the pressure on the wall. The computed wall shear stress, given by ρu_*^2, drops rapidly in the adverse pressure gradient region of the flow. Accompanying the sharp drop in the wall pressure, the wall shear stress rises steeply. With the final change of curvature of the streamlines at the tail, u_* drops almost to zero. The computed pressure distribution agrees well with the experimental data, having a maximum percentage difference of 1% of the total head $\rho U_o^2/2$. However, the computed u_* distribution by the parabolized method reaches a smaller value than the experimental data near the tail of the stern, being 25% under the experimental values at x/l = 0.97. The computed u_* and c_p distributions for Model 5 (Figures 3b and 3c) display the same type of behavior as exhibited for Model 1. Except the computed u_* distribution by the simple method has a higher value than the experimental data for x/L = 0.93. For Model 5, the agreement with the experimental data is good for both the wall frictional velocity and the wall pressure coefficient. As is evident by the steep drop in u_* in the adverse pressure gradient region of the flow, the flow about this body is very near to separation at x/L = 0.93. The computed u_* and wall c_p for flow past Model A are given in Figures 3b and 3c. As opposed to Afterbodies 1 and 5, the stern of Model A is not inflected. Therefore, over the aft region of the body, the pressure gradient remains adverse up to the tail of the body and u_* steadily decreases to zero. The computed wall pressure distribution lies slightly above the experimental pressure distributions of less than 3% at x/L = 0.95. The shape of Model B is characterized by a sharply sloping stern region (Figures 5a, 5b, and 5c). The values of the surface angles near 90° at the stern caused some numerical difficulty for the parabolized N.-S. computer code. However, good agreement of the computed wall pressure with the experimental data is obtained, with a maximum difference of less than 4% occurring at x/L = 0.95 (Figure 5c). The sharp decrease in u_* indicates that the flow is nearing separation as the body sharply turns downward at the tail (Figure 5b). The differences between the computed values of u_* and c_p by the parabolized N.-S. code and the simple viscous-inviscid interaction code are generally small except near the tail end of the stern.

Figures 2d, 3d, 4d, and 5d present detailed comparisons of the computed velocity fields to the experimental results for the four bodies. In Figure 2d, the computed velocity profiles show remarkable agreement with the experimental data for Model 1 up to the tail of the body. The computed velocities near the tail and in the wake are also in good agreement with the experimental results (Figure 2d). The largest discrepancy occurs immediately behind the body (x/L = 1.0076). Farther into the wake, the agreement with experiment is very good, as is evident by the profiles at x/L = 1.1820. Computed and experimental velocity profiles for Model 5 are presented in Figure 3d. The overall agreement with the experimental data is good. Figures 4d and 5d present the total velocity profiles for the flows past Models A and B. The agreement of the computed velocity fields with the experimental velocities is very good with a maximum difference of less than 2%. Detailed comparisons of the parabolized N.-S. calculations and the simple viscous-inviscid interaction computations for the four bodies are shown in Figures 2 through 5. For Model 1 (Figures 2b and 2c), the u_* and c_p distributions are in general agreement up to x/L = 0.95. The simple method does not predict as steep a drop in u_* at the concave part of the body as do the parabolized N.-S. calculations. In addition, there is no trough at the stern in the pressure distribution computed by the simple method (Figure 2c). The velocity profiles computed for Model 1 (Figure 2d) from the two methods are consistent. For Model 5, the parabolized N.-S. calculation correctly predicts the steep drop in u_* and the pressure trough near the tail end of the stern (Figure 3b). The velocity profile comparisons for Model 5 (Figure 3d) demonstrate again the agreement of the two methods (within 2%). The calculations for u_* and c_p for Model A (Figures 4b and 4c) demonstrate that the calculations agree up to the tail of the body. At the tail, the partially parabolic N.-S. calculation of the u_* distribution drops rapidly to zero as opposed to the simple method which shows a slight upturn. Both pressure distributions turn downward at the tail, with the parabolized N.-S. pressure distribution reaching a slightly higher maximum. The computed velocity profiles for Model A (Figure 4d) are again consistent. The comparisons of u_*, c_p, and velocity for Model B (Figures 5b and 5d) show the same behavior as demonstrated for Model A.

Figure 7 - (Continued)

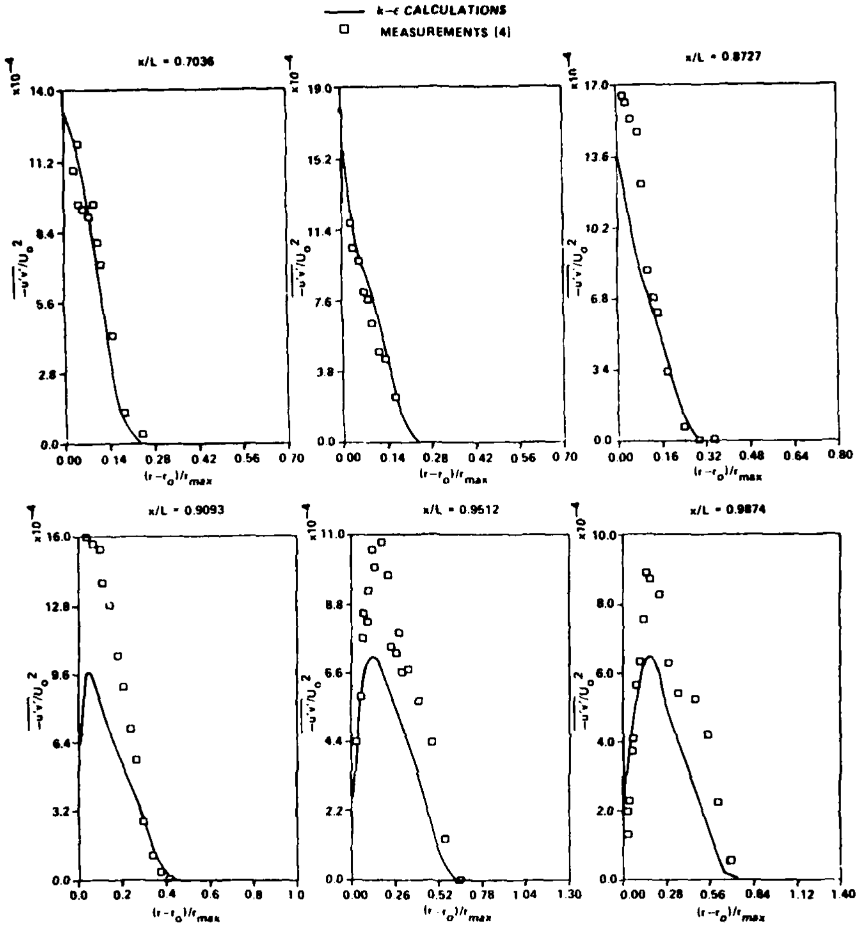

(b) DTNSRDC Axisymmetric Model 5

INITIAL DISTRIBUTION

Copies	
1	WES
1	U.S. ARMY TRAS R&D Marine Trans Div
3	ONR/432F Whitehead, Lee, Reischman
2	NRL
	1 Code 2027
	1 Code 2629
1	ONR/Boston
1	ONR/Chicago
1	ONR/New York
1	ONR/Pasadena
1	ONR/San Francisco
1	NORDA
3	USNA
	1 Tech Lib
	1 Nav Sys Eng Dept
	1 B. Johnson
3	NAVPGSCOL
	1 Lib
	1 T. Sarpkaya
	1 J. Miller
1	NOSC/Lib
1	NCSC/712
1	NCEL/131
1	NSWC, White Oak/Lib
1	NSWC, Dahlgren/Lib
1	NUSC/Lib

Copies	
11	NAVSEA
	1 SEA 99612 (Library)
	1 SEA 05R24 (J. Sejd)
	1 SEA 55W3 (E. Comstock)
	1 SEA 55W33 (W. Sandburg)
	1 SEA 55W31 (W. Louis)
	1 SEA 55W31 (G. Jones)
	1 SEA 55N2 (A. Paladino)
	1 SEA 55N1 (S.G. (Wieczorek)
	1 SEA 63R31 (T. Peirce)
	1 SEA 56X12 (C.R. Crockett)
	1 SEA 62R41 (L. Pasiuk)
1	NAVFAC/032C
1	NADC
1	NAVSHIPYD PTSMH/Lib
1	NAVSHIPYD PHILA/Lib
1	NAVSHIPYD NORVA/Lib
1	NAVSHIPYD CHASN/Lib
1	NAVSHIPYD LBEACH/Lib
2	NAVSHIPYD MARE
	1 Lib
	1 Code 250
1	NAVSHIPYD PUGET/Lib
1	NAVSHIPYD PEARL/Code 202.32
1	NAVSEC, NORVA/6660.03, Blount
12	DTIC
1	AFOSR/NAM
1	AFFOL/FYS, J. Olsen
2	MARAD
	1 Div of Ship R&D
	1 Lib

Copies	
1	NASA/HQ/Lib
3	NASA/Ames Res Ctr, Lib 1 D. Kwak 1 J.L. Steger 1 Lib
2	NASA/Langley Res Ctr 1 Lib 1 D. Bushnell
1	NBS/Lib
1	NSF/Eng Lib
1	LC/Sci & Tech
1	DOT/Lib TAD-491.1
2	MMA 1 National Maritime Res Ctr 1 Lib
3	U of Cal/Dept Naval Arch, Berkeley 1 Lib 1 W. Webster 1 R. Yeung
2	U of Cal., San Diego 1 A.T. Ellis 1 Scripps Inst Lib
1	U of Cal., Santa Barbara/Tulin
4	CIT 1 Aero Lib 1 T.Y. Wu 1 A.J. Acosta 1 D. Coles
1	California State University/ Cebeci
1	Catholic U of Amer/Civil & Mech Eng
1	Colorado State U/Eng Res Ctr
1	Cornell U/Shen

Copies	
2	Harvard U 1 G. Carrier 1 Gordon McKay Lib
1	U of Illinois/J. Robertson
4	U of Iowa 1 Lib 1 L. Landweber 1 V.C. Patel 1 C.J. Chen
1	Johns Hopkins U/Lib
4	MIT 1 Lib 1 J.R. Kerwin 1 T.F. Ogilvie 1 J.N. Newman
2	U of Minn/St. Anthony Falls 1 Lib 1 R. Arndt
1	U of Mich/NAME/Lib
1	U of Notre Dame/Eng Lib
1	New York U/Courant Inst/Lib
3	Penn State 1 B.R. Parkin 1 R.E. Henderson 1 ARL Lib
1	Princeton U/Mellor
1	U of Rhode Island/F.M. White
1	Science Application, Inc. Annapolis, MD C. von Kerczek
1	SIT/Lib
1	U of Texas/Arl Lib
1	Utah State U/Jeppson

Copies	
1	Southwest Res Inst 1 Applied Mech Rev
3	Stanford U 1 Eng Lib 1 R. Street, Dept Civil Eng 1 S.J. Kline, Dept Mech Eng
1	Stanford Res Inst/Lib
1	U of Virginia/Aero Eng Dept
1	U of Washington/Arl Tech Lib
1	U.S. Naval Academy
2	VPI 1 Dept Mech Eng 1 J. Schetz, Dept Aero & Ocean Eng
2	Webb Inst 1 Lib 1 Ward
1	Woods Hole/Ocean Eng
1	Worchester PI/Tech Lib
1	SNAME/Tech Lib
1	Bell Aerospace
1	Bethlehem Steel/Sparrows Point
1	National Science Foundation/ Eng Div Lib
1	Bethlehem Steel/New York/Lib
4	Boeing Company/Seattle 1 Marine System 1 P. Rubbert 1 G. Paynter 1 H. Yoshihara
1	Bolt, Beranek & Newman/Lib
1	Cambridge Acoustical Associates, Inc.

Copies	
1	Exxon, NY/Design Div/ Tank Dept
1	Exxon Math & System, Inc.
1	General Dynamics, EB/Boatwright
1	Flow Research
1	Gibbs & Cox/Tech Info
2	Grumman Aerospace Corp 1 Lib 1 R.E. Melnik
1	Hydronautics/Lib
1	Lockheed, Sunnyvale/Waid
1	Lockheed, California/Lib
1	Lockheed, Georgia/Lib
2	McDonnell Douglas, Long Beach 1 T. Cebeci 1 J.L. Hess
1	Newport News Shipbuilding/Lib
1	Nielsen Eng & Research
1	Northrop Corp/Aircraft Div
1	Rand Corp
1	Rockwell International 1 B. Ujihara
1	Sperry Rand/Tech Lib
1	Stanford Research Inst/Lib
1	Sun Shipbuilding/Chief Naval Arch
1	TRW Systems Group/Lib
1	TRACOR

Copies	
1	United Technology/East Hartford, Conn
2	Westinghouse Electric 1 M.S. Macovsky 1 Gulino
1	Woods Hole Oceanographic, Inc./ Ocean Eng Dept

CENTER DISTRIBUTION

Copies	Code	Name
1	1500	W.B. Morgan
1	1504	V.J. Monacella
1	1506	S. Hawkins
1	1508	R. Boswell
1	152	W.C. Lin
1	1521	W. Day
1	1522	C.C. Hsu
1	1522	M.B. Wilson
1	1522	C.H. Sung
1	154	J. McCarthy
1	154	P. Granville
1	1540.1	B. Yim
1	1540.2	R. Cumming
30	1542	T.T. Huang
1	1542	N.C. Groves
1	1542	G.S. Belt
1	1542	Y.T. Lee
1	1542	M.S. Chang
1	1542	R.W. Burke
1	1544	F. Peterson
1	156	D.S. Cieslowski
1	1561	G. Cox
1	1564	J. Feldman
1	1606	T.C. Tai
1	1802.1	H. Lugt
1	1840	J. Schot

Copies	Code	Name
1	1843	H. Haussling
1	19	M.M. Sevik
1	1905.1	W. Blake
1	194	F.S. Archibald
10	5211.1	Reports Distribution
1	522.1	TIC (C)
1	522.2	TIC (A)

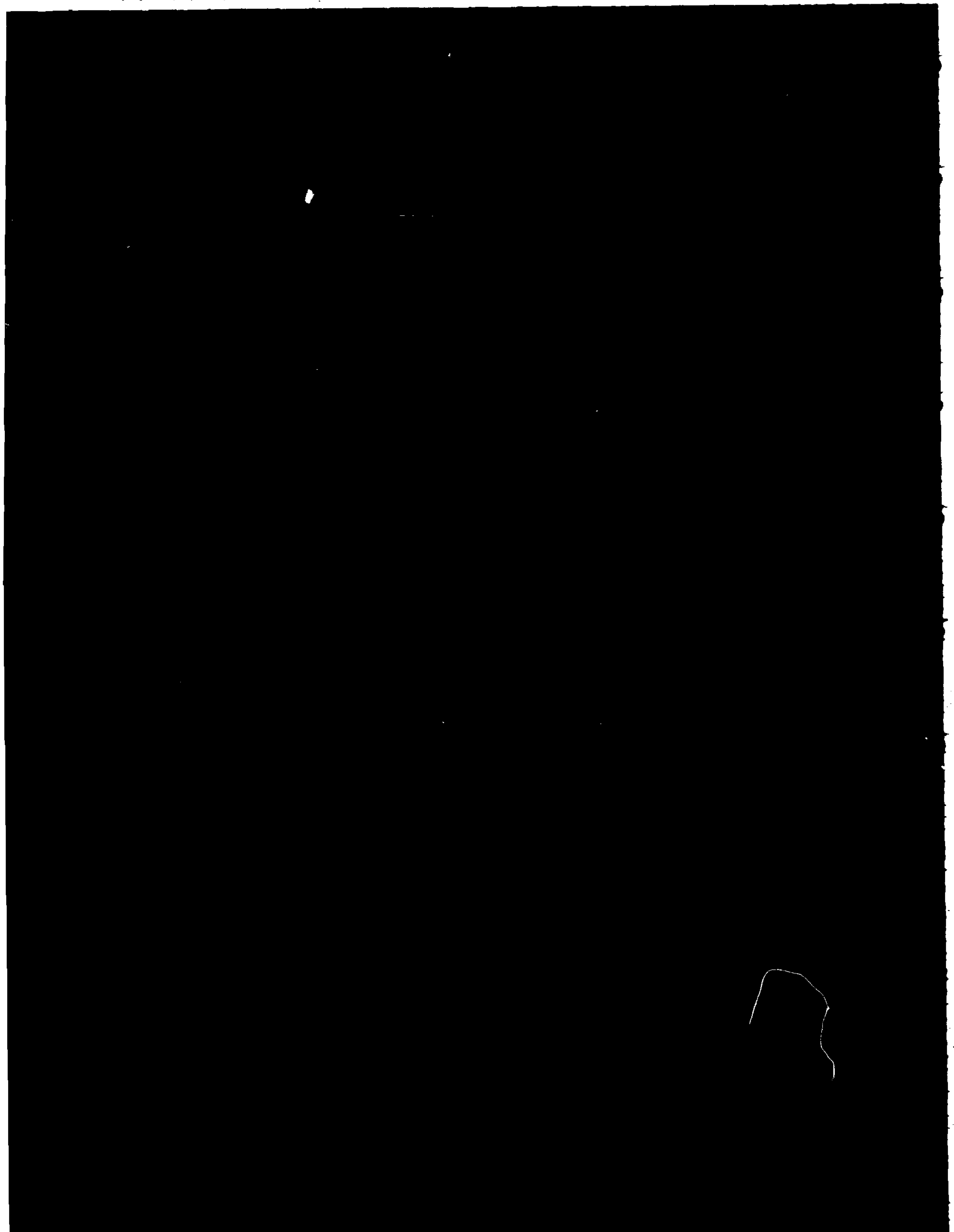

END

FILMED

5-85

DTIC